Anchoring intermediate phases via few-layer MoSSe nanosheets in flexible porous carbon fiber for stable lithium ion storage

Mengluan Gao[a], Zhe Cui[b], Jinqi Zhu[a], Rujia Zou*[a], Wenqing Wang[a], Ye Chen*[a] and Huifang Chen*[a]

a State Key Laboratory for Modification of Chemical Fibers and Polymer Materials, College of Materials Science and Engineering, Donghua University, Shanghai 201620, China

b Macao Institute of Materials Science and Engineering (MIMSE), Faculty of Innovation Engineering, Macau University of Science and Technology, Taipa, Macao 999078, China

*Corresponding authors.

E-mail addresses: rjzou@dhu.edu.cn (R. Zou), chenye@dhu.edu.cn (Y. Chen), hfchen@dhu.edu.cn (H. Chen).

Figure S1. Optical photographs of MoSSe/CNFs film.

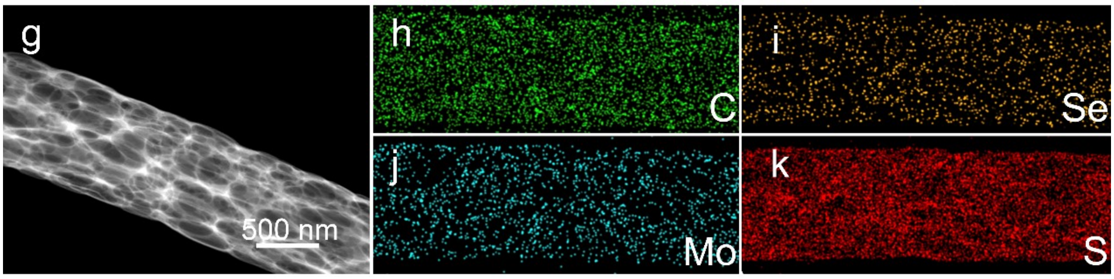

Figure S2. EDS mapping of MoSSe/CNFs.

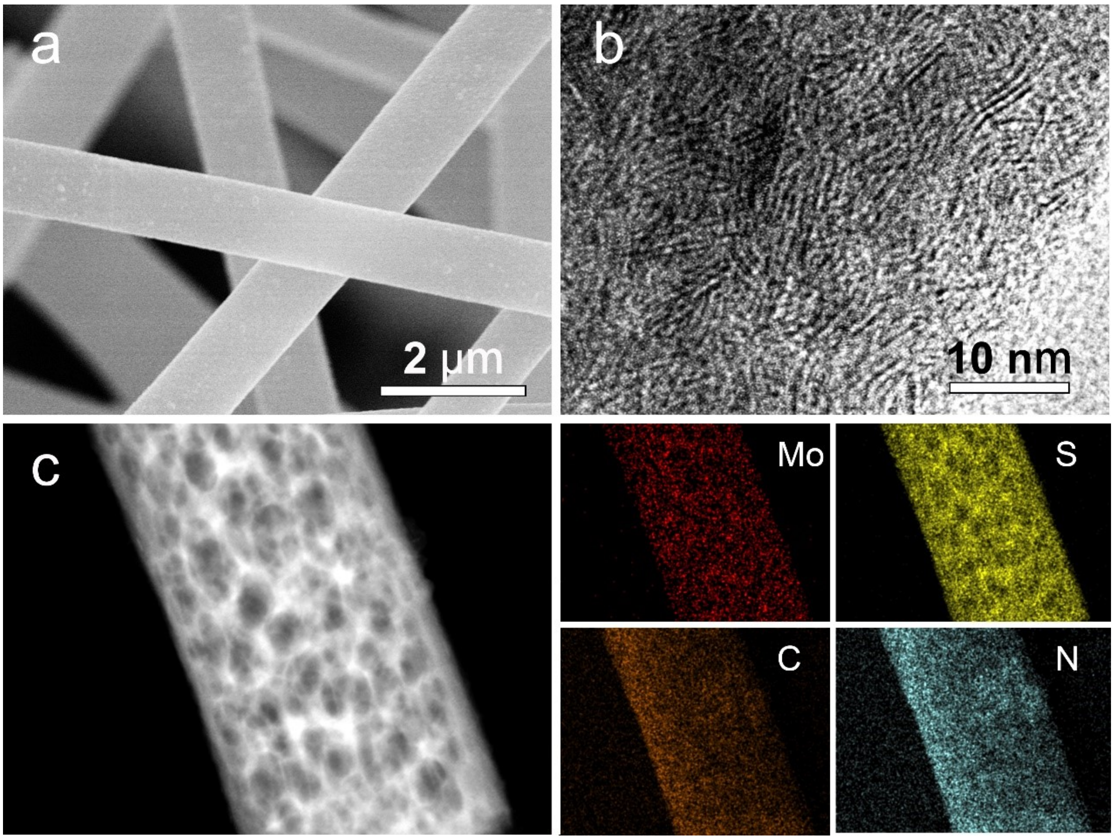

Figure S3. a) SEM image, b) HRTEM image and c) EDS mapping of MoS2/CNFs.

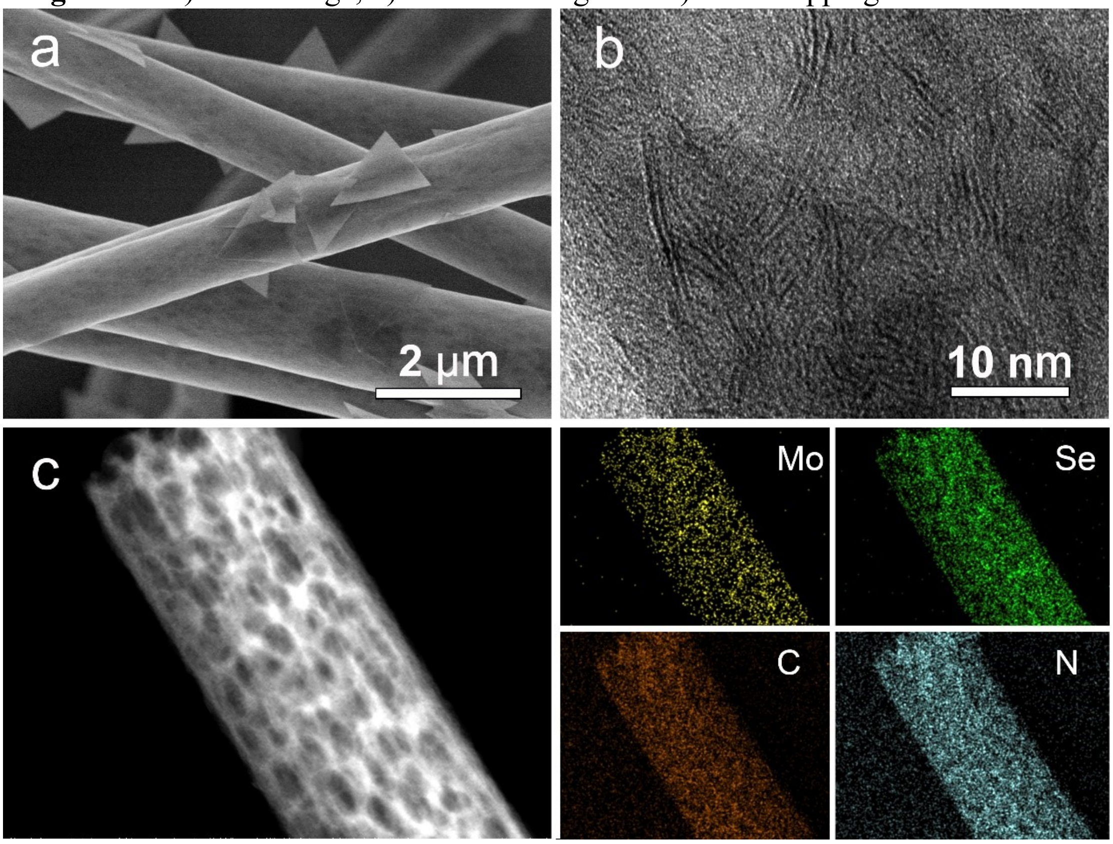

Figure S4. a) SEM image, b) HRTEM image and c) EDS mapping of MoSe2/CNFs.

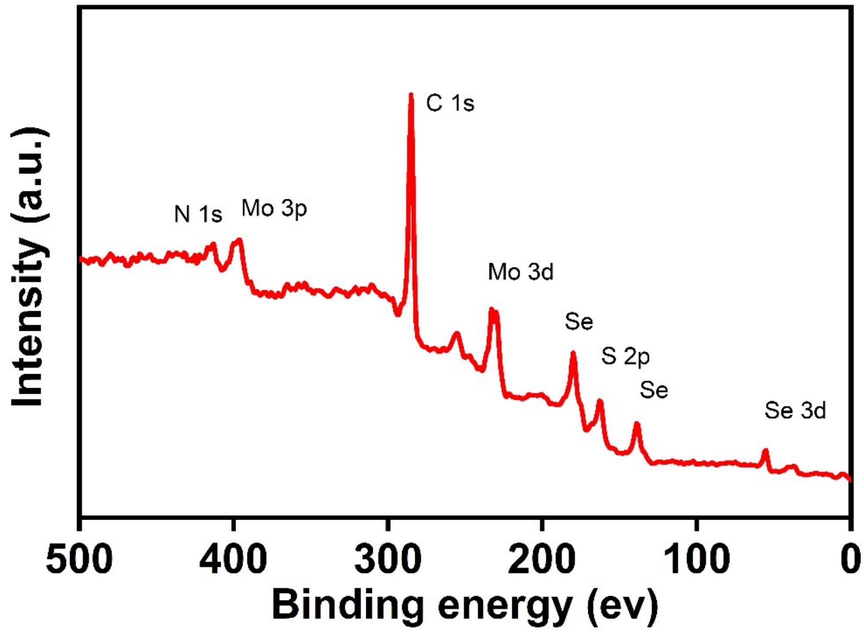

Figure S5. The XPS survery spectrum of MoSSe/CNFs.

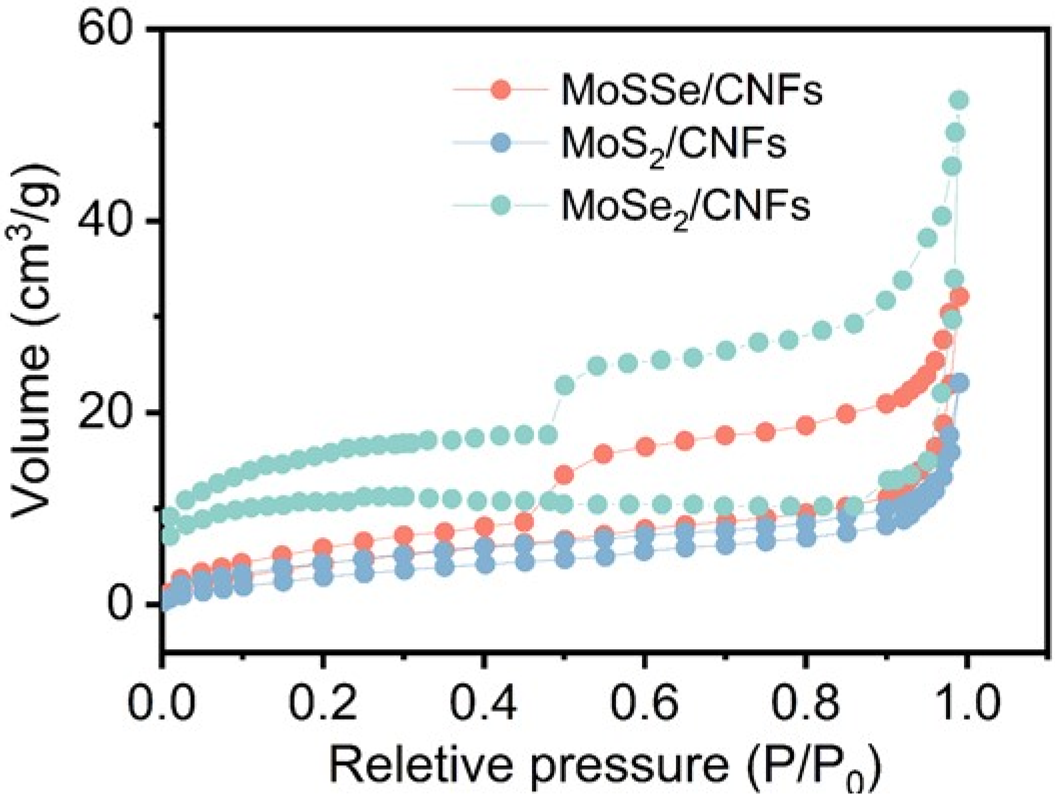

Figure S6. N2 adsorption－desorption isotherm of MoSSe/CNFs, MoS_2/CNFs and $MoSe_2$/CNFs.

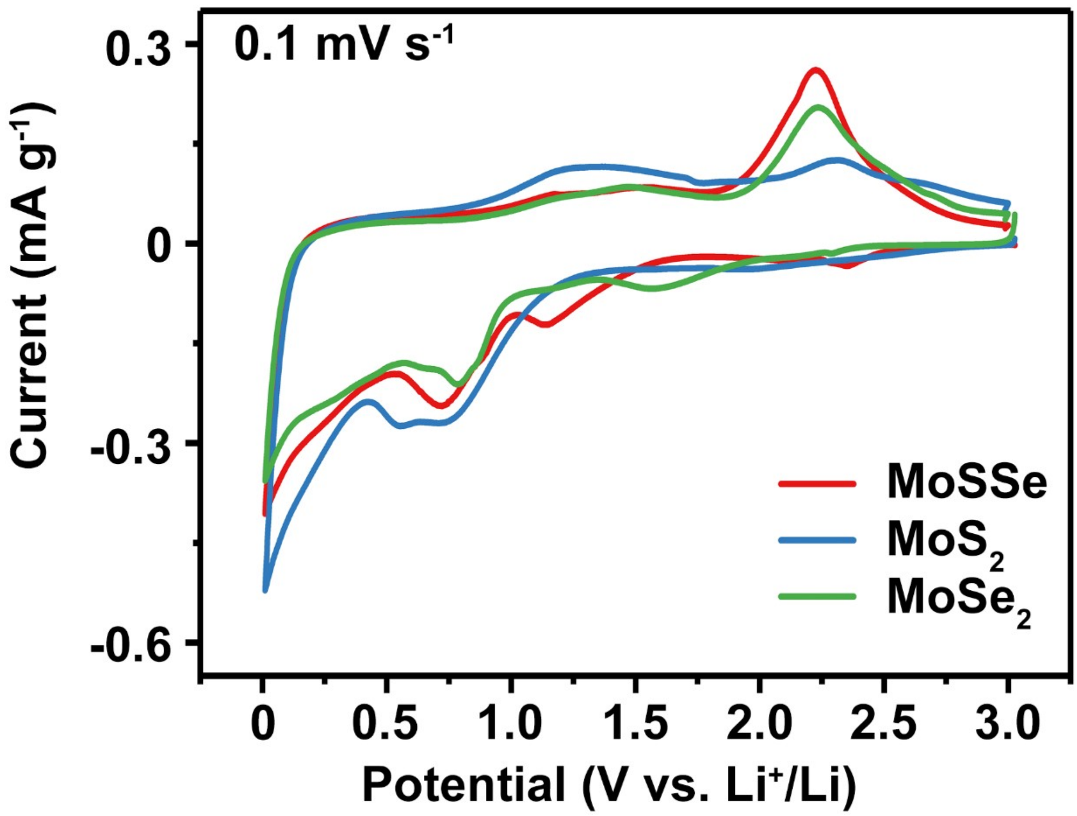

Figure S7. CV curves at 0.1 mV s^{-1} the initial cycle of MoSSe/CNFs, MoS_2/CNFs and $MoSe_2$/CNFs.

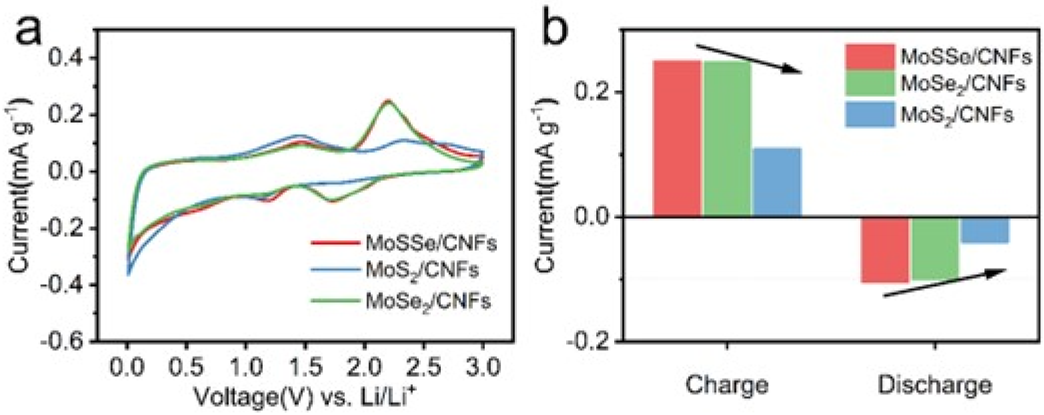

Figure S8. a) CV curves at 0.1 mV s^{-1} the second cycle of MoSSe/CNFs, MoS_2/CNFs and $MoSe_2$/CNFs. b) Comparison graph of peak currents for MoSSe/CNFs, MoS_2/CNFs and $MoSe_2$/CNFs.

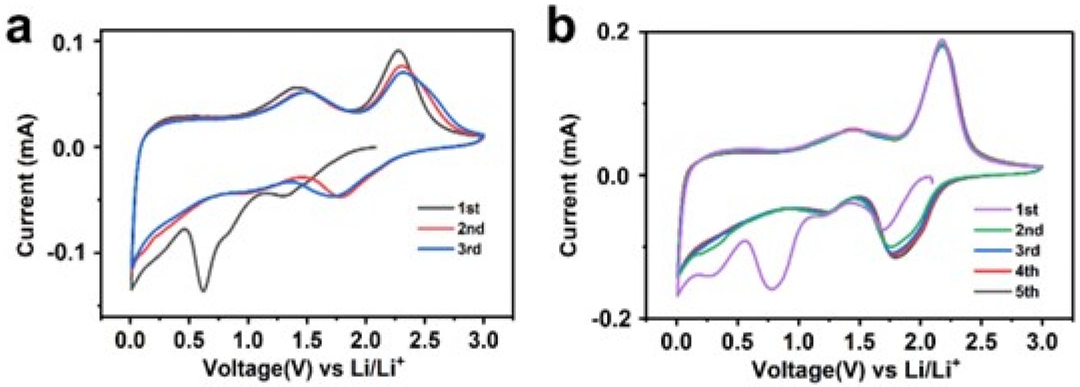

Figure S9. a) CV curves of MoS_2/CNFs at 0.1 mV s^{-1} scan rate. b) CV curves of $MoSe_2$/CNFs at 0.1 mV s^{-1} scan rate.

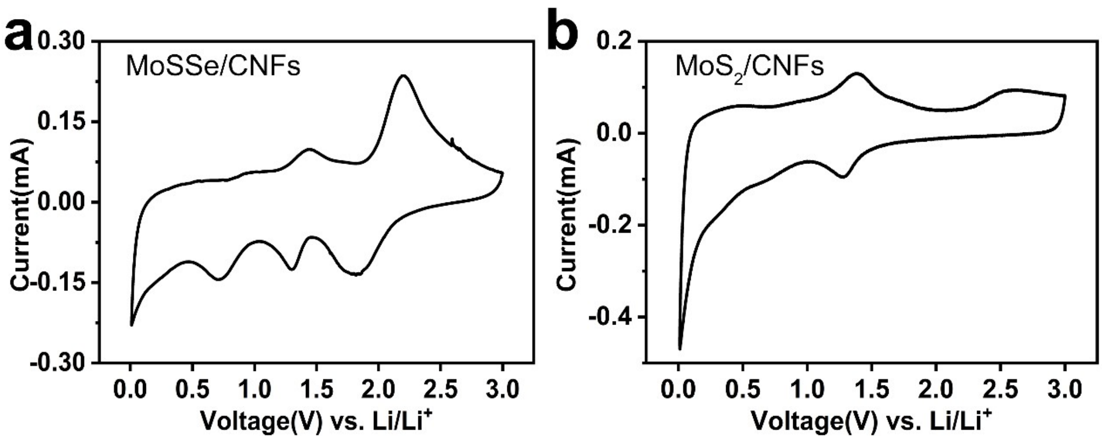

Figure S10. a) CV curves of MoSSe/CNFs at 0.2 mV s^{-1} scan rate after 200 cycles at 5 A g^{-1}. b) CV curves of MoS_2/CNFs at 0.2 mV s^{-1} scan rate after 200 cycles at 5 A g^{-1}.

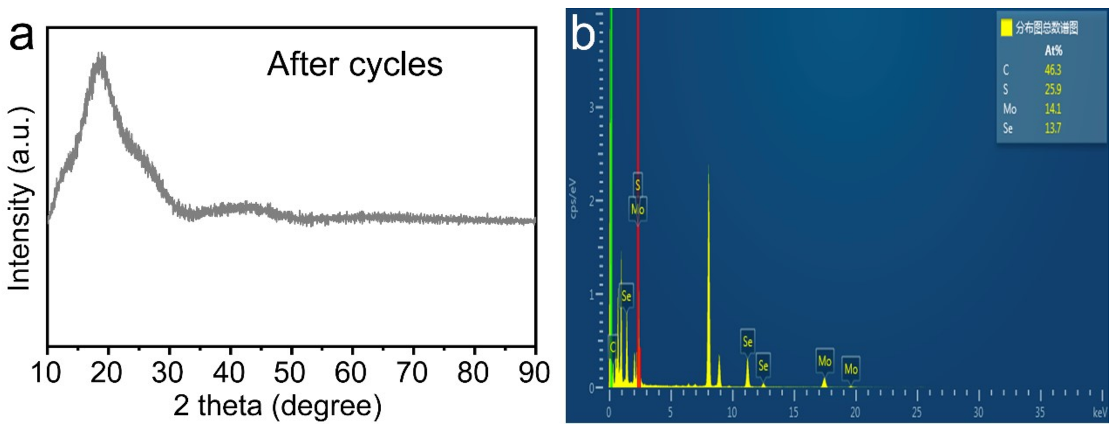

Figure S11. a) Elemental compositions of MoSSe/CNFs at fully delithiated to 3 V versus Li^+/Li by EDS analysis. b) XRD patterns of MoSSe/CNFs electrode after cycling.

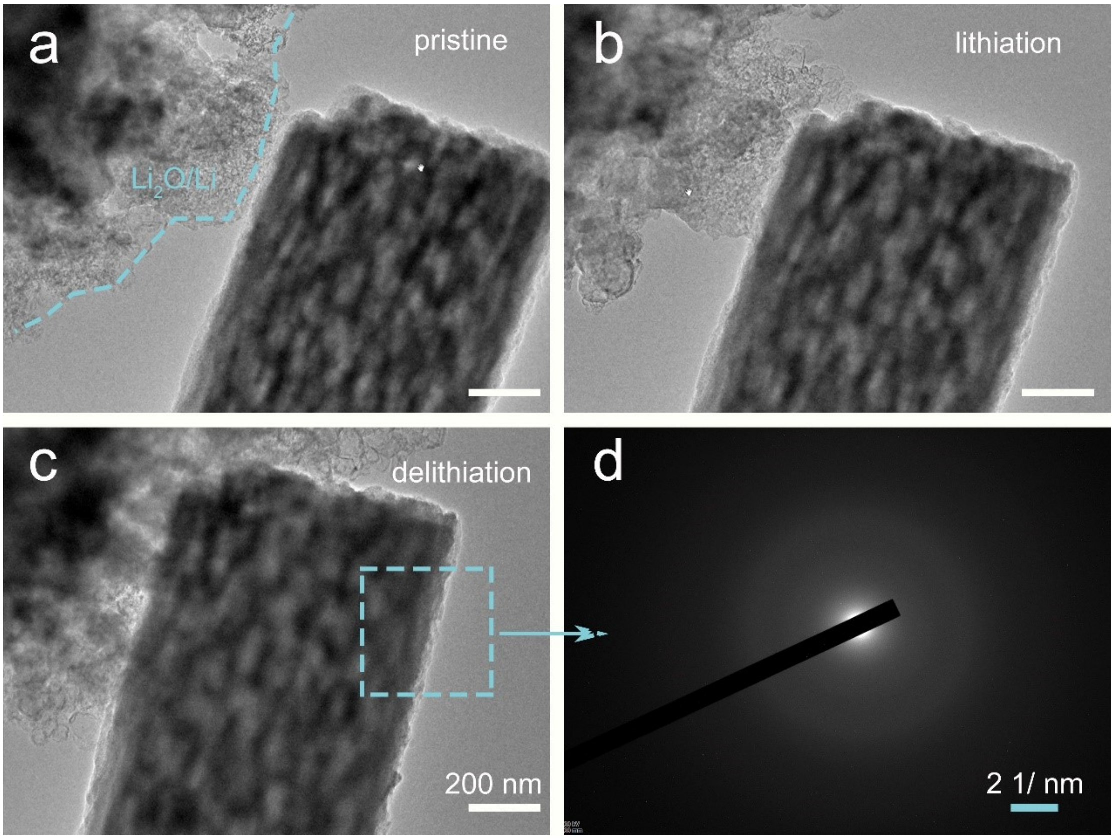

Figure S12. a-c) TEM images of MoSSe/CNFs during in situ lithiation/delithiation processes in TEM. d) Selected area electron diffraction (SAED) patterns for after first cycle.

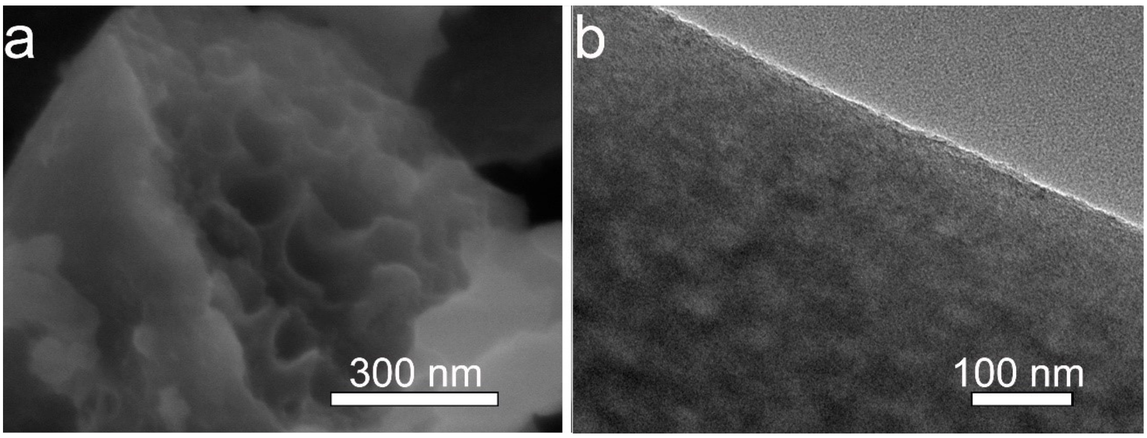

Figure S13. a) SEM, b) TEM images of MoSSe/CNFs electrode after cycling.

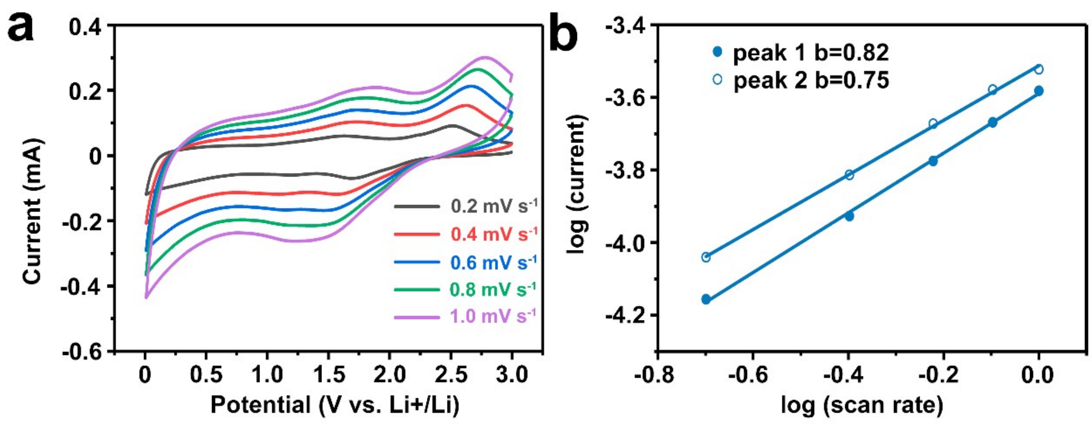

Figure S14. a) CV curves of MoS_2/CNFs at scan rates from 0.2 to 1.0 mV s^{-1}. b) Corresponding liner relationship between log (i) and log (v) of different peaks.

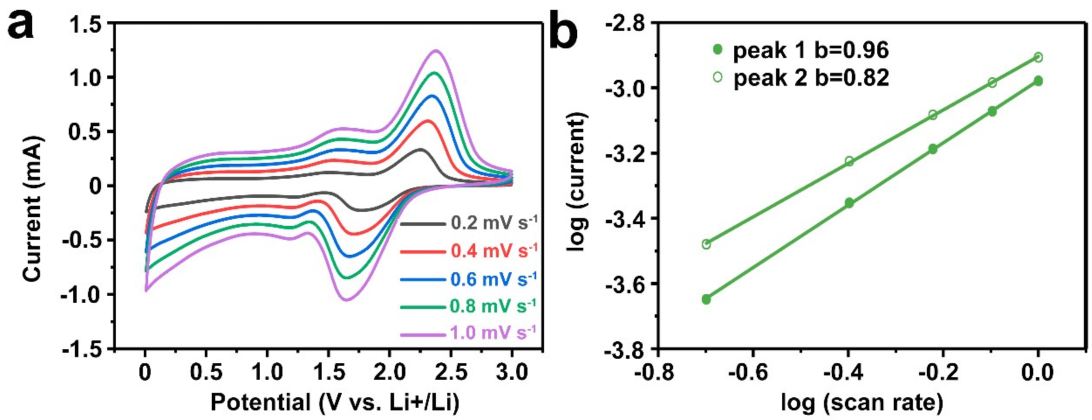

Figure S15. a) CV curves of $MoSe_2$/CNFs at scan rates from 0.2 to 1.0 mV s^{-1}. b) Corresponding liner relationship between log (i) and log (v) of different peaks.

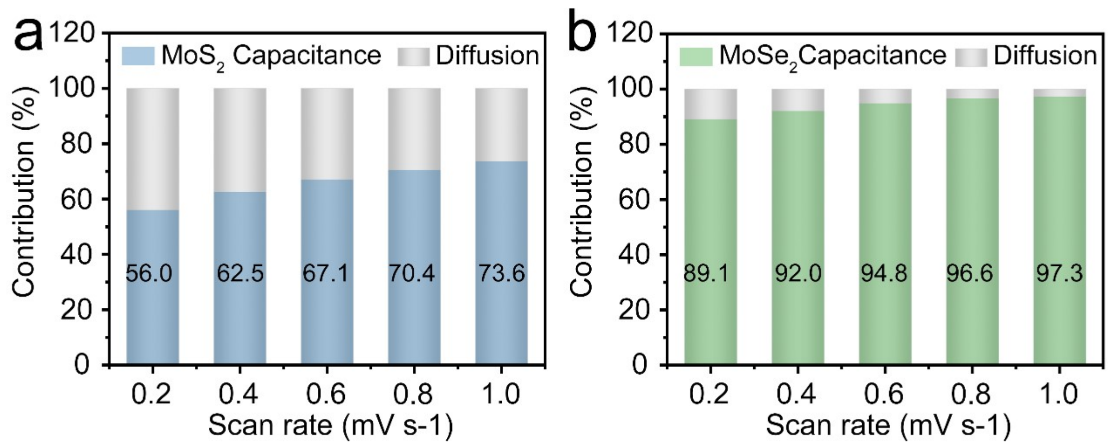

Figure S16. Contribution ratio of the capacitive process at different scan rates for a) MoS_2, and b) $MoSe_2$.

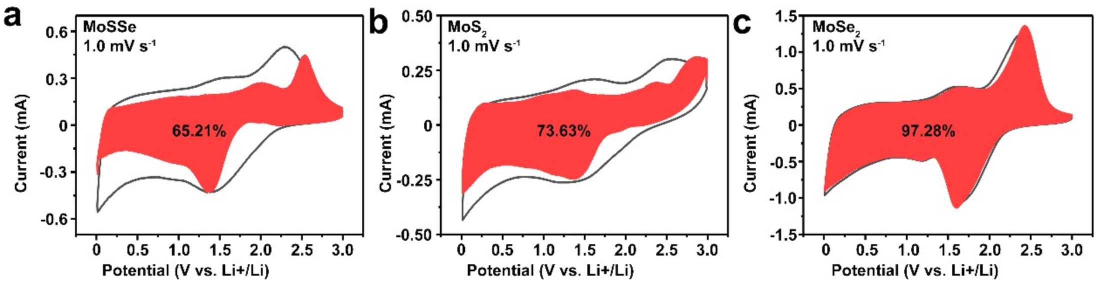

Figure S17. CV curves of the capacitive contribution at 1.0 mV s^{-1}.

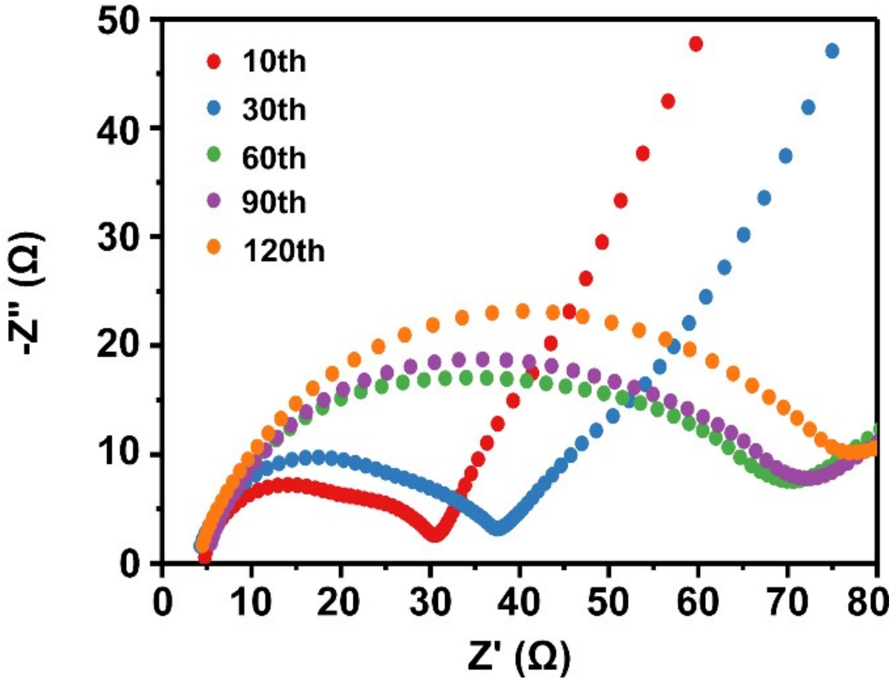

Figure S18. EIS spectra of MoS_2/CNFs electrodes with different cycles.

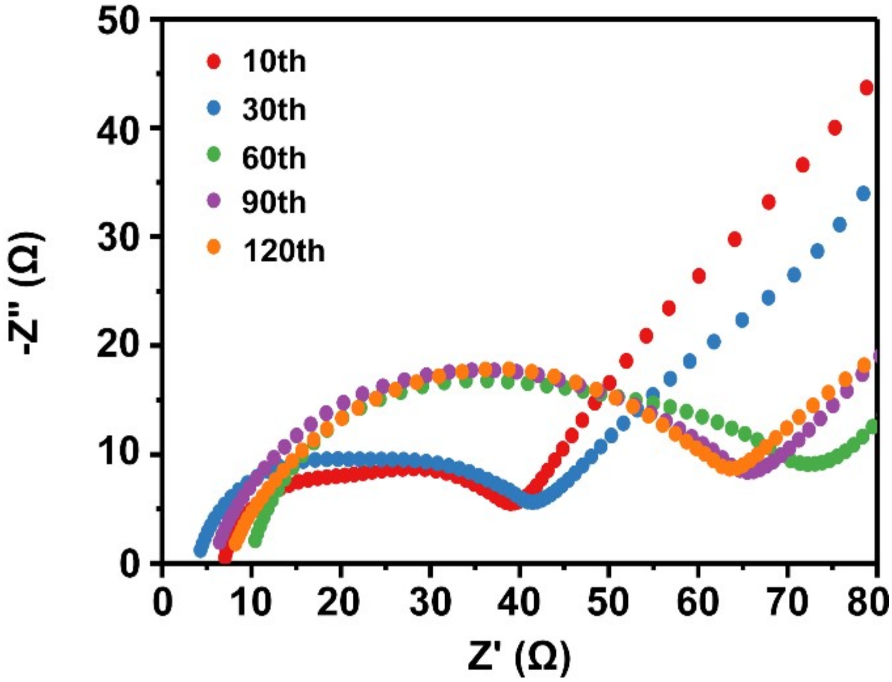

Figure S19. EIS spectra of $MoSe_2$/CNFs electrodes with different cycles.

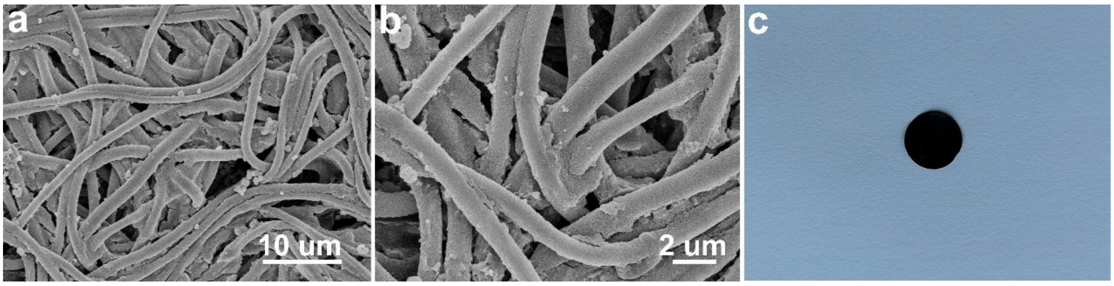

Figure S20. SEM images and optical photographs of MoSSe/CNFs after cycling.

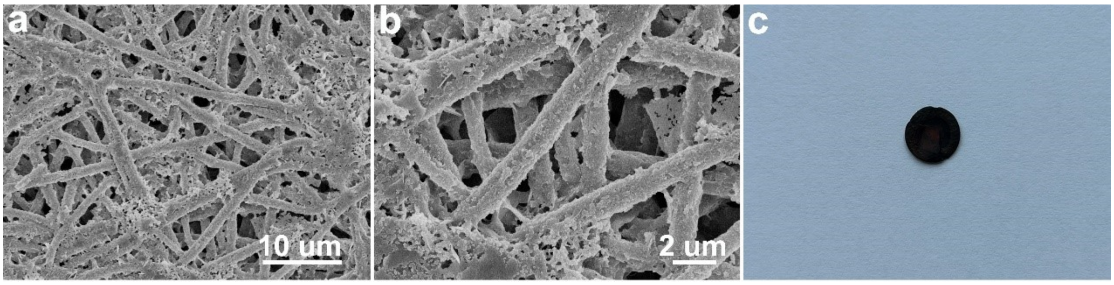

Figure S21. SEM images and optical photographs of MoS_2/CNFs after cycling.

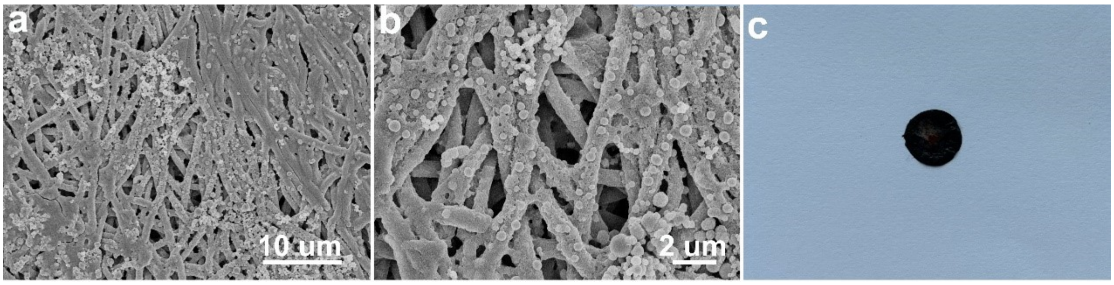

Figure S22. SEM images and optical photographs of $MoSe_2$/CNFs after cycling.

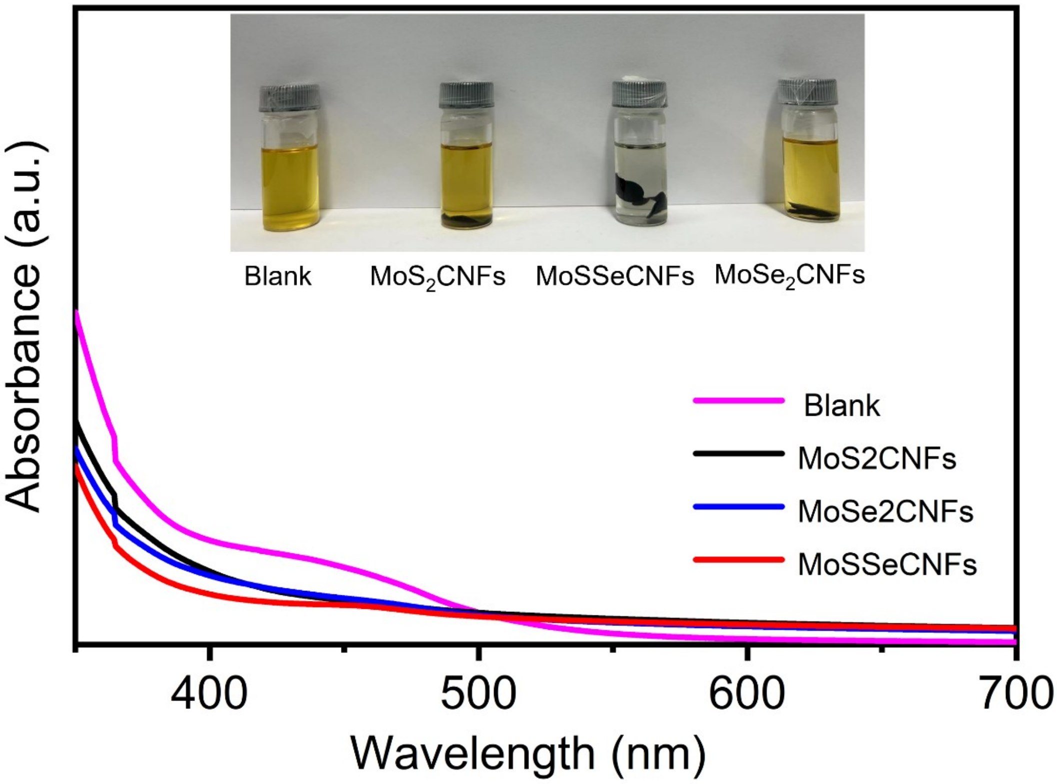

Figure S23. UV-Vis spectra of polysulfide solution upon adsorption by different sorbents.

Table S1. Raman spectra parameters of as-prepare products.

Products	D1 band	D3 band	D4 band	G band	I_{D1}/I_G
MoSSe/CNFs	1356	1532	1201	1601	1.42
$MoSe_2$/CNFs	1321	1435		1593	1.25
MoS_2/CNFs	1359	1515		1599	1.31

Table S2. The comparison of molybdenum- or selenide-based or sulfide-based anode materials recently.

Materials	Rate performance	Cyclic performance	Reference
CoP-C@MoS_2/C	945.5 mAh g^{-1} at 0.1 A g^{-1} 484.9 mAh g^{-1} at 0.1 A g^{-1}	460 at 5 A g^{-1} for 2000 cycles	[1]
CoS_2@NC-400	1024.6 mAh g^{-1} at 0.2 A g^{-1} 463.3 mAh g^{-1} at 2 A g^{-1}	767.6 at 0.5 A g^{-1} for 500 cycles	[2]
NiS/SnO_2/MOF	932 mAh g^{-1} at 0.05 A g^{-1} 400 mAh g^{-1} at 2 A g^{-1}	430 at 2 A g^{-1} for 1000 cycles	[3]
MXene@MoS_2	817 mAh g^{-1} at 0.2 A g^{-1} 717 mAh g^{-1} at 10 A g^{-1}	877 at 1 A g^{-1} for 70 cycles	[4]
MoS_2/Fe_2O_3 @CNF-3	1060 mAh g^{-1} at 0.05 A g^{-1} 443 mAh g^{-1} at 5 A g^{-1}	559.74 at 1 A g^{-1} for 500 cycles	[5]
Cu_2S@NSC	610.4 mAh g^{-1} at 0.1 A g^{-1} 387.6 mAh g^{-1} at 5 A g^{-1}	512.7 at 1 A g^{-1} for 1000 cycles	[6]

$NbSe_2$@PPy-2	819 mAh g^{-1} at 0.1 A g^{-1} 361 mAh g^{-1} at 4 A g^{-1}	670 at 0.5 A g^{-1} for 210 cycles	[7]
$MoO_2/Cu_{2-x}Se$@C	667.5 mAh g^{-1} at 0.1 A g^{-1} 285.2 mAh g^{-1} at 5 A g^{-1}	480.9 at 2 A g^{-1} for 500 cycles	[8]
$MoSe_2$/rGO	770 mAh g^{-1} at 0.1 A g^{-1} 560 mAh g^{-1} at 2 A g^{-1}	732.9 at 1 A g^{-1} for 300 cycles	[9]
MoO_2/N-MCNTs	833.4 mAh g^{-1} at 0.5 A g^{-1} 523.7 mAh g^{-1} at 3 A g^{-1}	507.8 at 1 A g^{-1} for 500 cycles	[10]
MoSSe/CNFs	996.9 mAh g^{-1} at 0.2 A g^{-1} 616.8 mAh g^{-1} at 10 A g^{-1}	750 at 5 A g-1 for 950 cycles	**This work**

Table S3. Values of Rs, Rf and Rct obtained from the fitting date.

Electrodes	R_s (Ω)	R_f (Ω)	R_{ct} (Ω)
MoSSe/CNFs	4.546	36.24	102.4
$MoSe_2$/CNFs	2.252	48.64	237.4
MoS_2/CNFs	10.65	32.08	418.1

References:

[1] Y. Xia, T. Yang, Z. Wang, T. Mao, Z. Hong, J. Han, D.L. Peng, G. Yue, Van der Waals forces between S and P ions at the CoP-C@MoS_2/C heterointerface with enhanced lithium/sodium storage, Adv. Funct. Mater. 33 (2023) 2302830. https://doi.org/10.1002/adfm.202302830.

[2] J. Xu, P. Ye, Y. Cheng, L. Ji, Y. Wei, Y. Chen, Meta-organic framework-based CoS_2 nitroge-doped carbon for high-performance lithium storage, Energy Technol-Ger 11 (2023) 2201452. https://doi.org/10.1002/ente.202201452.

[3] N. Zhang, Q. Meng, H. Wu, X. Hu, M. Zhang, A. Zhou, Y. Li, Y. Huang, L. Li, F. Wu, R. Chen, Co-MOF as stress-buffered architecture: an engineering for improving the performance of NiS/SnO_2 heterojunction in lithium storage, Adv. Energy Mater. (2023). https://doi.org/10.1002/aenm.202300413.

[4] H. Tan, L. Zhang, K. Gao, L. Sun, Y. Zhang, F. Xie, Few-layer MoS_2 nanosheets vertically supported on Ti_3C_2-MXene sheets promoting lithium storage performance, Dalton T. 52 (2023) 16413-16420. https://doi.org/10.1039/d3dt01963b.

[5] X. Chen, Q. Zhang, H. Wang, L. Wang, H. Wang, Y. Zeng, MoS_2 nanoflowers implanted in nitrogen-doped carbon fibers with Fe_2O_3 nanoparticles decorated for enhanced lithium storage performance, J. Alloys Compd. 963 (2023). https://doi.org/10.1016/j.jallcom.2023.171195.

[6] T. Li, D. Zhao, M. Shi, T. Wang, Q. Yin, Y. Li, J. Qi, F. Wei, Y. Sui, MOF-derived N,S Co-doped carbon matrix-encapsulated Cu_2S nanoparticles as high-performance lithium-ion battery anodes: a joint theoretical and experimental study, J. Mater. Chem. A 11 (2023) 1461-1472. https://doi.org/10.1039/d2ta08539a.

[7] B.-H. Kang, S. Shin, K. Nam, J. Bae, J.-M. Oh, S.-M. Koo, H. Sohn, S.-H. Park, W.H. Shin, Exfoliated $NbSe_2$ nanosheet@polypyrrole hybrid nanocomposites as a high performance anode of lithium-ion batteries, J. Mater. Chem. A 11 (2023) 19083-19090. https://doi.org/10.1039/d3ta01335a.

[8] M. Zhong, X. Guo, L. Li, Y.-W. Li, K. Zhao, H. Peng, X. Zhang, Hetero-phase $MoO_2/Cu_{2-x}Se$ nanocomposites distributed in porous octahedral carbon networks for high-performance lithium

storage, ACS Appl. Nano Mater. 6 (2023) 20018-20027. https://doi.org/10.1021/acsanm.3c03824.
[9] W. Wang, J.-Y. Chen, J. Ouyang, H. Yin, A.-J. Li, L. Chen, J.-L. Huang, Y.-C. Zhu, G.-Y. Li, Z.-H. Hou, Spray pyrolysis-derived W-doped $MoSe_2$/rGO paper-like microspheres: optimization of microstructure and mesostructure for enhanced lithium storage, Rare Met. 43 (2024) 3019-3031. https://doi.org/10.1007/s12598-024-02662-4.
[10] Z. Wang, X. Chen, D. Wu, T. Zhang, G. Zhang, S. Chu, B. Qian, S. Tao, Strong metal oxide-support interaction in MoO_2/N-doped MCNTs heterostructure for boosting lithium storage performance, J. Colloid Interface Sci. 650 (2023) 247-256. https://doi.org/10.1016/j.jcis.2023.06.192.